Chapter 1

Synthesis & Characterization of

SiW_{11} as well as

SiW_{11} anchored to MCM-41 (SiW_{11}/MCM-41)

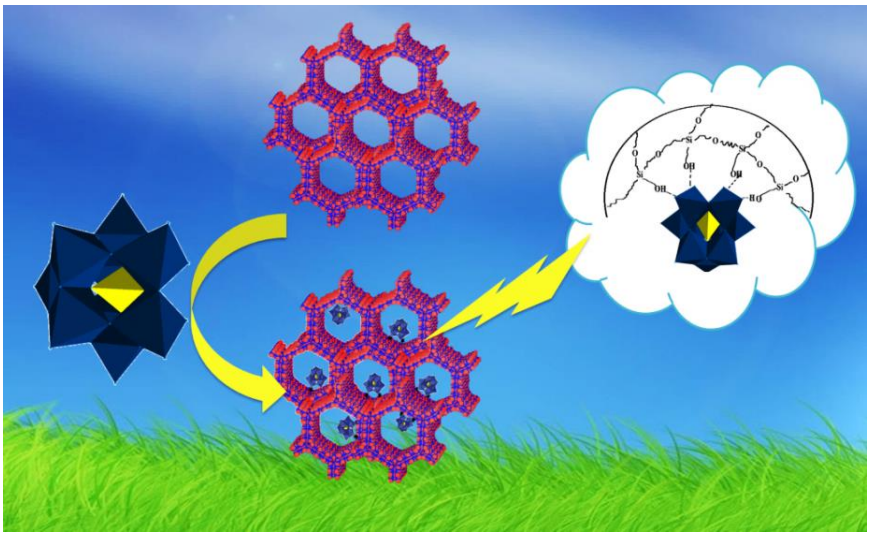

As mentioned earlier, although SiW_{12} as well as SiW_{12} anchored to MCM-41 was synthesized and characterized by our group earlier [1], here we have included the synthesis as well as characterization of SiW_{12}/MCM-41 once again in order to make comparison.

SYNTHESIS

Sodium salt of SiW_{11} was synthesized from individual salts, sodium tungstate and sodium silicates, as shown in Figure 1.

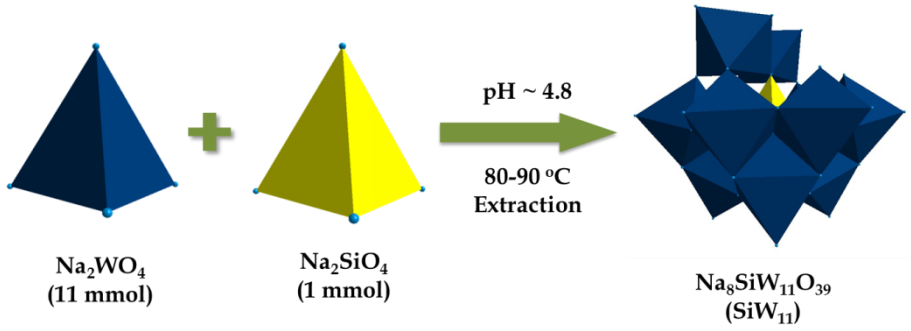

Figure 1. Synthesis of SiW_{11}.

Different methodologies have been employed for synthesis of anchored lacunary silicotungstates. Lefebvre et al. reported review covering synthesis of inorganic hybrid materials with encapsulated silicotungstates [2]. Hu and co-workers reported synthesis, characterization and photo-catalytic application of mono-lacunary silicotungstates based macroporous composite TiO_2 [3]. Same group reported a preparation of monolacunary silicotungstate (SiW_{11}) based SiO_2 composite films [4] and ordered macroporous hybrid SiO_2 materials [5] via sol-gel method. Their photocatalytic activity was evaluated for degradation of aqueous formic acid and aqueous malic acid respectively. Yang, et al. reported synthesis of monolacunary silicotungstate functionalized mesoporous hybrid SBA-15 [6] via sol-gel method. Very recently Cunha-Silva et al. reported synthesis of hybrid composite material, SiW_{11}@MIL-101, by the inclusion of the

potassium salt of mono-lacunary silicotungstates into the porous Metal-Organic Framework MIL-101(Cr) by post synthesis grafting method [7].

The synthesis of anchored LPOMs by sol-gel method is more complex and difficult, in which various synthetic conditions are required according to the silicon source and surfactant. POM species may be unstable or unable to interact with the surface under such conditions. Moreover, the introduction of bulky POMs may be unfavorable for the assembly of surfactant micelles so that no ordered mesostructure is formed in the synthesis. In order to overcome these possibilities, it was thought of interest to develop simple and easy synthesis method. Here we are reporting an impregnation method for the same.

The present chapter describes synthesis and physicochemical and spectroscopic characterization of catalyst SiW_{11} anchored to MCM-41. For comparison, characterization of SiW_{12} anchored to MCM-41 has also been included. The support and the catalysts were characterized by elemental analysis (EDS), thermo gravimetric analysis (TGA), Fourier Transform Infrared Spectroscopy (FT-IR), Laser-Raman Spectroscopy, X-ray diffraction (XRD), surface area measurement (BET method), pore size, pore volume and ^{29}Si MAS-NMR (Magic-Angle Spinning- Nuclear Magnetic Resonance) studies. Further, the surface morphology of support and catalysts was studied by Scanning Electron Microscopy (SEM) and Transmission Electron Microscopy (TEM). The strength as well as type of acidic sites was determined by n-butylamine potentiometric titrations.

EXPERIMENTAL

Materials

All materials used were of A.R. (analytical) grade. Silicotungstic acid, tetraethylorthosilicate (TEOS), sodium tungstate, sodium silicate, n-butylamine and acetone were purchased from Merck and used as received.

Synthesis of the support (MCM-41)

MCM-41 was synthesized using non-hydrothermal procedure reported by Cai, et al. [8] with slight modification. 1g Surfactant (CTAB) was added to the dilute solution of NaOH (2 M, 3.5 mL NaOH in 480 mL distilled water) with stirring at room temperature. After the solution became clear, 5 mL TEOS was added drop wise and the gel was aged for 2 h at 60 ^{o}C. The resulting material was filtered, washed with distilled water, dried in oven and calcined in air at 550 ^{o}C for 5 h. The obtained material was designated as MCM-41.

Synthesis of monolacunary silicotungstate, $Na_8SiW_{11}O_{39}$* $11H_2O$ (SiW_{11})

The mono lacunary silicotungstate was synthesized by following the method reported by Brevard et al. [9]. 0.22 mol, 7.2 g sodium tungstate and 0.02 mol, 0.56 g sodium silicate were dissolved in 150 mL distilled water at 80 ^{o}C. The pH was then adjusted to 4.8 by dilute nitric acid. The volume of the mixture was reduced to half and the resulting solution was filtered to remove unreacted silicates. The lacunary polyoxometalate anion was separated by liquid-liquid extraction with acetone. The extraction was repeated until the acetone extract showed the absence of nitrate ions. The extracted sodium salt of mono lacunary silicotungstate was dried at room temperature in air. The resulting material was designated as SiW_{11}.

Synthesis of the catalysts

Silicotungstic acid anchored to MCM-41 (SiW_{12}/MCM-41) [1]

SiW_{12} was anchored to MCM-41 by impregnation method. 1g of MCM-41 was impregnated with an aqueous solution of SiW_{12} (0.1g/10 mL of distilled water). The water from the suspension was allowed to evaporate at 100 °C in an oven. Then the resulting mixture was dried at 100 °C with stirring for 10h. The material thus obtained was designated as 10% SiW_{12}/MCM-41. Same procedure was followed for the synthesis of a series of SiW_{12} anchored catalyst (0.2-0.4 g/20-40 mL of distilled water). The obtained materials were designated as 20% SiW_{12}/MCM-41, 30% SiW_{12}/MCM-41 and 40% SiW_{12}/MCM-41, respectively.

Monolacunary silicotungstate anchored to MCM-41 (SiW_{11}/MCM-41)

SiW_{11} was anchored to MCM-41 by impregnation method. 1g of MCM-41 was impregnated with an aqueous solution of SiW_{11} (0.1g/10 mL of distilled water). The water from the suspension was allowed to evaporate at 100 °C in an oven. Then the mixture was dried at 100 °C with stirring for 10h. The obtained material was treated with 0.1 N HCl, filtered, washed with distilled water and dried at 100 °C. The material thus obtained was designated as 10% SiW_{11}/MCM-41. Same procedure was followed for the synthesis of a series of SiW_{11} anchored catalyst (0.2-0.4 g/20-40 mL of distilled water). The obtained materials were designated as 20% SiW_{11}/MCM-41, 30% SiW_{11}/MCM-41 and 40% SiW_{11}/MCM-41, respectively.

CHARACTERIZATION

Characterization is a central aspect of catalyst development [10-12]. The elucidation of the structures, compositions, and chemical properties of both, the supports used in heterogeneous catalysis as well as the active species present on the surfaces of the supported catalysts are very important for a better understanding of the relationship between catalyst properties and catalytic performance [12].

In case of supported catalysts, it is crucial to know if the active ingredient is on the surface of the support or diffuse in it. As a result from the scientific point of view, the investigation of the surface composition as well as local structure of catalyst at the atomic level and the correlation of these data with catalyst performance is very important in the catalytic reaction. The basic information on the structure-catalytic property relationship for catalyst systems will ultimately be of value in the design of new efficient catalysts [13]. Heterogeneous catalyst can be characterized by various tools which comprise different physicochemical and spectroscopic techniques that are summarized in block diagram shown in Figure 2.

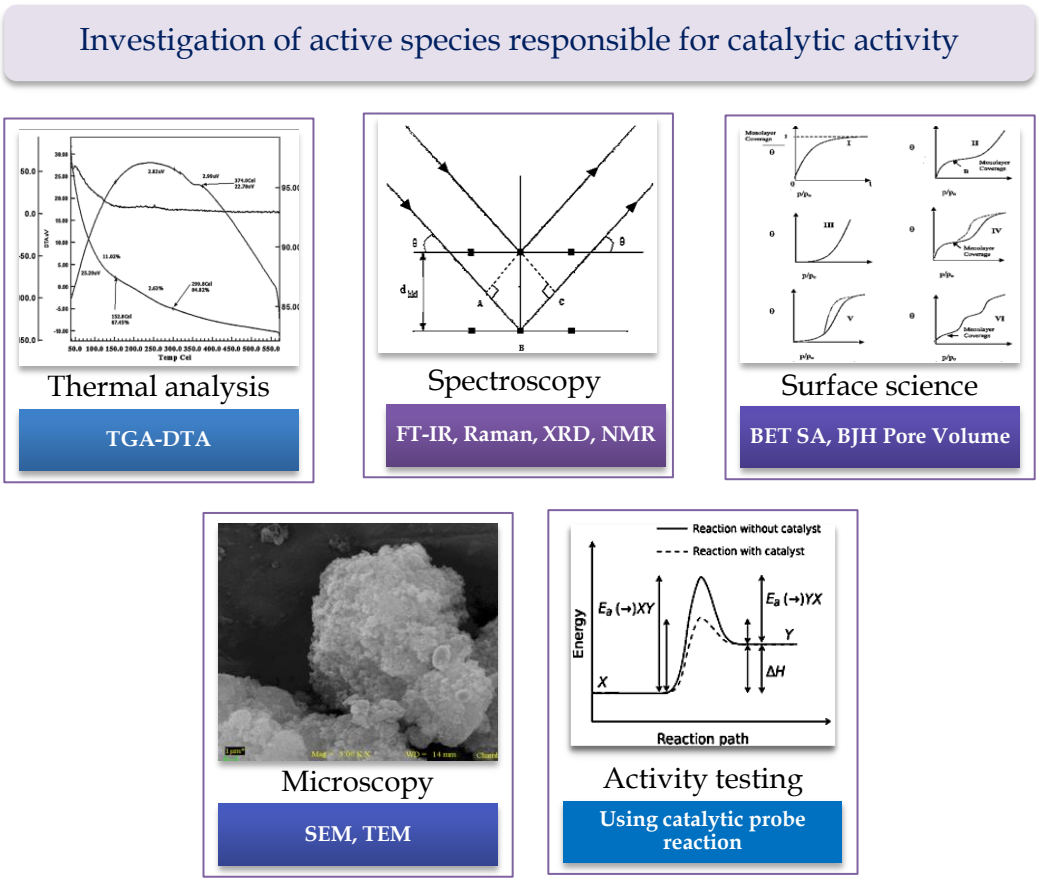

Figure 2. Depiction of various techniques used in characterization of catalyst.

During the last few years many techniques for determining chemical composition, electronic properties and the structure of the upper atomic layers of solids have reached maturity.

The available analytical techniques can be classified into broad categories based on the information obtained by them.

- Spectroscopic methods which include the study of structural aspects of the supported species as well as stability of supported species.
- Study of surface area, pore volume, particle diameter, particle size distribution, dispersion of the catalyst species as well as any structural change of supported species onto the surface of the support.

Spectroscopy is a non-destructive method of analysis and provides information on the types of atoms present on surfaces, how are they influenced by adsorbed species, precise adsorption sites of atoms and molecules, their bond strengths, lengths and angles, and the influence of surface chemical bond on surface reactivity.

In the present chapter, support and the catalysts were characterized by various physicochemical techniques such as EDS, TGA, FT-IR, Laser-Raman Spectroscopy, N_2 adsorption-desorption, ^{29}Si-MAS NMR, XRD, SEM and TEM. The types as well as strength of acidic sites were determined by n-butylamine potentiometric titration.

Elemental Analysis

Energy-dispersive X-ray spectroscopy (EDS or EDX) [14]

EDS or EDX is an analytical technique used for the elemental analysis or chemical characterization of a sample. It relies on the investigation of a sample through interactions between electromagnetic radiation and matter, analyzing X-rays emitted by the matter in response to being hit with charged particles. Its characterization capabilities are due in large part to the fundamental principle that each element has a unique atomic structure allowing X-rays that are characteristic of an element's atomic structure to be identified uniquely from one another.

The elemental analysis was carried out using JSM 5610 LV combined with INCA instrument for EDX-SEM analyzer for the quantitative identification of metal ions.

Thermo Gravimetric Analysis (TGA) [15]

It is a technique whereby the weight of a substance, in an environment heated or cooled at a controlled rate, is recorded as a function of time or temperature.

The temperature-weight loss profile of a supported catalyst can provide important quantitative information on the types of water present in the sample. It is usually possible to distinguish loosely held "physisorbed" water from strongly bonded "chemisorbed" water and helps determine the best conditions for removing the former.

More usefully, the study of the decomposition of less stable catalysts can also be done which help in determine the maximum activation temperatures and the temperatures at which the supported reagents can be safely used in reactions.

TGA measurements were carried out on the Mettler Toledo Star SW 7.01 in the temperature range 40 ^{o}C to 600 ^{o}C. All measurements were carried out under nitrogen atmosphere with a flow rate of 2 ml/ min and a heating rate of 10 ^{o}C/ min.

Fourier Transform Infrared Spectroscopy (FT-IR) [14]

FT-IR spectroscopy is probably the most useful and widely used technique to study supported reagents. It provides the following information.

1. Identification of the surface species
2. Dispersion of the reagent over the support surface
3. Surface activity studies with the use of probe molecules

The most common ways of studying an insoluble solid are: 1) as a mull; 2) as a disc; and 3) directly as a powder. These methods differ in terms of degree of difficulty (in obtaining useful spectra), ease of sample preparation, and

reliability of the information obtained. Both the mull and disc methods are transmittance techniques. FT-IR opaque or highly scattering materials may not be suitable for analysis by transmission spectroscopy.

FT-IR absorption spectra of various catalysts were recorded on a FT-IR Perkin Elmer instrument at room temperature using KBr pellets in the range of 4000 cm^{-1} to 400 cm^{-1}. The powdered samples were ground with KBr in 1: 10 ratio and pressed (5 ton/cm^2) for making the pellets. The data were collected at an average of 25 scans.

FT- Raman spectroscopy (LRS) [16]

Raman spectroscopy (named after Sir C. V. Raman) is a spectroscopic technique used to study vibrational, rotational, and other low-frequency modes in a system. It relies on inelastic scattering, or Raman scattering, of monochromatic light, usually from a laser in the visible, near infrared, or near ultraviolet range.

Most Raman spectrometers for material characterization use a microscope to focus the laser beam to a small spot (< 1-100 mm diameter). Light from the sample passes back through the microscope optics into the spectrometer. Raman shifted radiation is detected with a charge-coupled device (CCD) detector, and a computer is used for data acquisition and curve fitting. These factors have helped Raman spectroscopy to become a very sensitive and accurate technique.

The Raman spectra were recorded on a FT-Raman Spectrophotometer Model Bruker FRA 106.

Solid state MAS-NMR (^{29}Si) [17]

In nuclear magnetic resonance, Magic Angle Spinning (MAS) is a technique often used to perform experiments in solid-state NMR spectroscopy.

By spinning the sample (usually at a frequency of 1 to 70 kHz) at the magic angle θ_m (ca. 54.74°, where $\cos^2\theta_m=1/3$) with respect to the direction of the magnetic field, the normally broad lines become narrower, increasing the resolution for better identification and analysis of the spectrum.

The chemical shifts of peaks in solid state ^{29}Si NMR spectra were used for characterization of solid materials. The magic- angle spinning (MAS) solid state NMR studies was carried out on a Bruker Avance DSX-300 NMR spectrometer under ambient conditions. The ^{29}Si NMR spectra were recorded at 121.49 MHz using a 7 mm rotor probe, number of acquisitions AQ: 0.0048888 Sec and spinning rate of 5-7 kHz, with TMS as an external standard.

Powder X-Ray Diffraction (XRD) [14]

XRD can be used to detect poorly dispersed or macro-crystalline reagent. In principle, XRD can be used to give quick information on the efficiency of dispersion of any supported reagent where the reagent normally exists in the crystalline state. XRD may also be useful for the identification of species formed during the preparation on subsequent chemistry of a supported reagent. This can be especially useful for unstable reagents, corrosive reagents and where the supported reagent has been subject to high-temperature thermal treatment. XRD has also been used to characterize the nature of surface species.

The powder X Ray Diffraction pattern of support and the catalysts was obtained by using the instrument Philips Diffractometer (Model PW - 1830). The conditions used were Cu Kα radiation (1.5417 Å), scanning angle from 0° to 80°.

BET Measurement [15]

As surface area of the catalyst is directly proportional to the catalytic activity of the heterogeneous catalysts, the measurement of the surface area is most important study for the same. Further from the surface area, one can get the information on the pore volume, pore size which will be helpful to understand the mechanism of the reaction occurs.

Apart from surface area measurements, determination of pore size distribution is an equally important parameter. For a given catalyst, the distribution of pore sizes may be such that some of the catalyst is completely inaccessible to large molecules and may restrict the rate of conversion of products by controlling the diffusion of reactant in the internal pore structure. The standard method for measuring catalyst areas and pore size are based on the physical adsorption of gas on the solid surface.

Surface area and pore size distribution of various catalysts were measures according to Brunauer-Emmett-Teller (BET) method, involving nitrogen adsorption-desorption using Micromeritics Surface area Analyzer (Model: ASAP 2020). From the adsorption desorption isotherms specific surface area was calculated using BET method. The samples were degassed under vacuum (5 – 10.3 mmHg) at 150 °C for 4 h, prior to measurement, to evacuate the physisorbed moisture. Further the pore size distributions were calculated applying the Barrett-Joyner-Halenda (BJH) method to the desorption branches of the isotherm.

Scanning Electron Microscopy (SEM) [14]

SEM provides morphological and topological information about the surfaces of solids that is usually necessary in understanding the behavior of the surfaces. The surface of a solid sample is swept in a raster pattern with a finely focused

beam of electrons or with a suitable probe. The surface morphology of the support and the anchored POMs were studied.

SEM has been used successfully to study reagent dispersion and surface morphologies. SEM can prove to be more sensitive technique than XRD to study reagent dispersion.

The surface morphology of the supports as well as catalysts was studied by Scanning Electron Microscopy using a JEOL SEM instrument (Model-JSM-5610 LV) with scanning electron electrode at 15 kV. Scanning was done at 1 mm range and images taken at a magnification of 100X for ZrO_2 and 100X and single particle image at 500X for the catalysts.

Transmission Electron Microscopy (TEM) [18]

TEM images are formed using transmitted electrons (instead of the visible light) which can produce magnification details up to 1,000,000 x with resolution better than 10 A^o. The images can be resolved over a fluorescent screen or a photographic film. Furthermore the analysis of the X-ray produced by the interaction between the accelerated electrons with the sample allows determining the elemental composition of the sample with high spatial resolution.

TEM was done on JEOL (JAPAN) TEM instrument (model-JEM 100CX II) with accelerating voltage 220 kV. The samples were dispersed in ethanol and ultra-sonicated for 5-10 minutes. A small drop of the sample was then taken in a carbon coated copper grid and dried before viewing.

Acidity measurement

A complete description of the surface acid properties of a solid involve the determination of the acid strength of the sites, their density (number of acid

centers per unit surface area of the solid), and their nature (Bronsted or Lewis type). Such descriptions are not easy to make, as the strength and the density of the sites are generally strictly connected to each other and besides the distribution of the acid strength is usually heterogeneous.

A small quantity (0.1 mL) of 0.05 N, n-butylamine in acetonitrile was added to a suspension of 0.5 g of the catalyst in 50 mL of acetonitrile and the system was stirred at 25 ^{o}C. Then, the suspension was potentiometrically titrated against 0.05 N, n-butylamine in acetonitrile. The electrode potential variation was measured with a digital pH meter.

The acidity of the catalyst measured by this technique allows us to evaluate the total number of acid sites as well as their acidic strength. In order to interpret the results, it is suggested that the initial electrode potential (Ei) indicates the maximum acid strength of the surface sites and the range where the plateau is reached (meq/g solid) indicates the total number of acid sites [19].

RESULTS AND DISCUSSION

Characterization of SiW_{12}

SiW_{12} was characterized by various physicochemical techniques in our previous publication [1].

Characterization of SiW_{11}

Elemental Analysis (EDS)

Table 1. EDS elemental analysis of SiW_{11}.

Elements	SiW_{11}	
	Analytical (%)	Observed (%)
W	66.3	63.8
Si	0.9	0.89
Na	6.02	6.0
O	26.4	29.3

The isolated sodium salt of SiW_{11} was dried and subjected to EDS elemental analysis. Table 1 show the % of elements by analytically calculated as well as observed EDS elemental analysis. The observed values for the elemental analysis are in good agreement with the theoretical values indicating the formation of SiW_{11}.

Thermal Analysis

The TGA of SiW_{11} (Figure 3) shows the preliminary weight loss of ~ 6-7% from 30-130 ^{o}C. This is due to the removal of adsorbed water molecules. Second weight loss of 2-2.5% up to 230 ^{o}C may be due to loss of water of

crystallization. The steady weight loss after 330 ^{o}C indicates the decomposition of SiW_{11} species.

DTA of SiW_{11} (Figure 3) shows endothermic peaks at 110 ^{o}C and 170 ^{o}C, due to the loss of adsorbed water and water of crystallization, respectively. In addition, DTA of SiW_{11} also shows a broad exothermic peak in the region of 330-420 ^{o}C due to the decomposition of SiW_{11}.

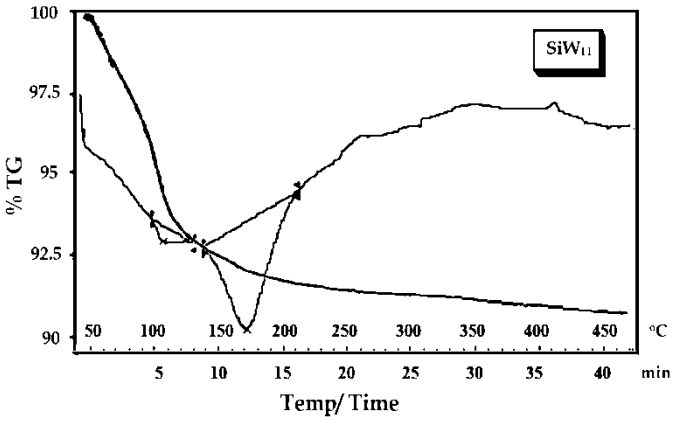

Figure 3. TG-DTA thermogram of SiW_{11}.

Number of water molecules was determined from the TGA curve using the following formula,

$$18\,n = \left(\frac{X\,[M + 18\,n]}{100}\right)$$

Where, n = number of water molecules, X = % loss from TGA and M = molecular weight of substance (without water of crystallization)

Based on studies the chemical formula of the isolated sodium salt was proposed as,

$$\boldsymbol{Na_8[SiW_{11}O_{39}].11\,H_2O}$$

Fourier Transform Infrared Spectroscopy (FT-IR)

The FT-IR spectra of SiW_{12} and SiW_{11} are presented in Figure 4. FT-IR spectrum of SiW_{12} has four characteristic bands at 1020, 926, 878, and 779 cm^{-1} corresponding to $W=O_d$ asymmetrical, $Si-O_a$ asymmetrical, $W-O_b-W$ asymmetrical, and $W-O_c-W$ asymmetrical respectively. Where O_a, O_b, O_c, and O_d attributed to the oxygen atoms connected to silicon, to oxygen atoms bridging to two tungsten (from two different triads for O_b and from the same triad for O_c), and to the terminal oxygen W=O, respectively [20].

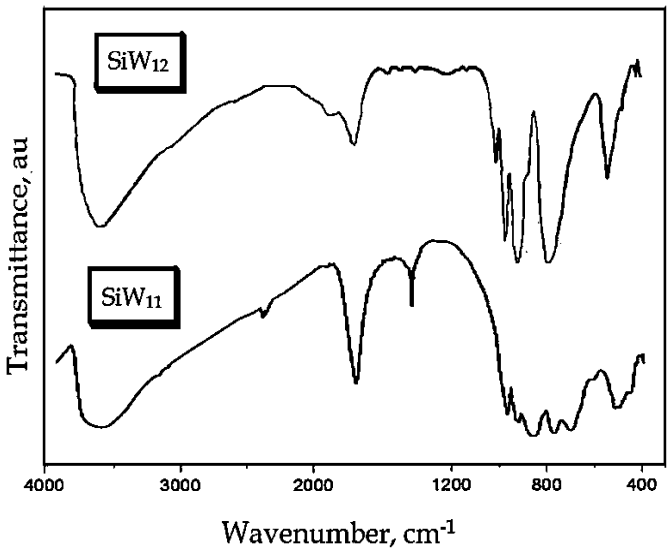

Figure 4. FT-IR spectra for SiW_{12} and SiW_{11}.

The FT-IR of SiW_{11} (Figure 4) shows bands at 987 cm^{-1} ($W=O_d$), 948 cm^{-1} ($Si-O_a$), 886 and 795 cm^{-1} ($W-O_b-W$) and 727 cm^{-1} ($W-O_c-W$). These bands are in good agreement with the reported one [21]. Observed splitting for $W-O_b-W$ band in SiW_{11} as compared to that of SiW_{12} is due to the lowering in the symmetry from Td (SiW_{12}) to Cs (SiW_{11}) around central heteroatom, Silicon. The result confirms the formation of SiW_{11}.

FT- Raman Spectroscopy

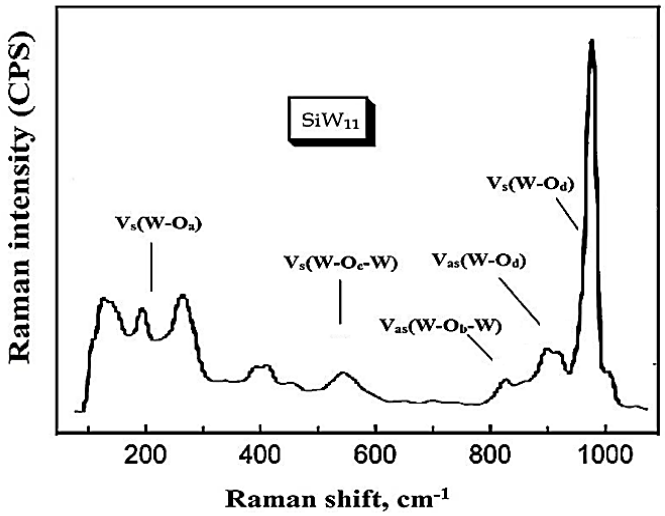

Figure 5. FT-Raman spectrum of SiW_{11}.

FT-Raman of SiW_{12} showed bands at 1054, 976, 888, 565 and 208 which were attributed to $\nu_s(W{=}O_d)$, $\nu_{as}(W{=}O_d)$, $\nu_{as}(W\text{-}O_b\text{-}W)$, $\nu_s(W\text{-}O_c\text{-}W)$, and $\nu_s(W\text{-}O_a)$, respectively [1]. The Raman spectrum of SiW_{11} shows retention of typical bands at 971, 890, 814, 521 and 231 cm^{-1} corresponding to υ_s $(W\text{-}O_d)$, υ_{as} $(W\text{-}O_d)$, υ_{as} $(W\text{-}O_b\text{-}W)$, υ_s $(W\text{-}O_c\text{-}W)$, and υ_s $(W\text{-}O_a)$, respectively (Figure 5). The presence of these bands confirms the formation of lacunary SiW_{11} species.

^{29}Si MAS- NMR studies

^{29}Si MAS-NMR is the most important technique to study chemical environment around the silicon nuclei in silica materials. The ^{29}Si MAS-NMR spectrum of SiW_{11} (Figure 6) shows signal at -84.68 ppm which is in quite good agreement with reported one [22]. The single sharp peak confirms the formation of single, un-fragmented species, SiW_{11}.

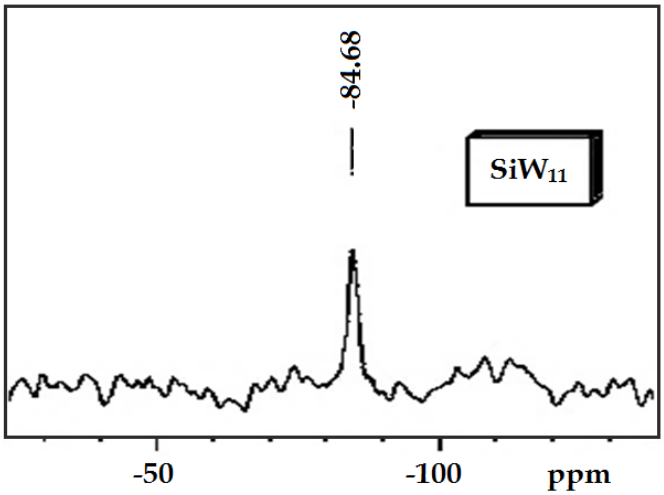

Figure 6. ^{29}Si MAS-NMR spectrum of SiW_{11}.

Thus, the thermal as well as spectral studies confirm the formation of SiW_{11}.

Characterization of SiW_{12}/MCM-41 [1] as well as SiW_{11}/MCM-41

Leaching Test

Leaching is a negative property for any catalyst. Any leaching of the catalyst from the support would make the catalyst unattractive. So, it is necessary to study the stability of polyanion onto support in order to reuse the catalyst. When the polyoxometalate react with a mild reducing agent such as ascorbic acid [23], it develops blue coloration, which can be used for the quantitative characterization for the leaching of polyoxometalate from the support. In the current work, we have used this method for determining the leaching of SiW_{12}/SiW_{11} from MCM-41 support.

Standard samples amounting to 1-5% of SiW_{12}/SiW_{11} in water were prepared. To 10 mL of the above samples, 1 mL of 10% ascorbic acid was added. The mixture was diluted to 25 mL. The resultant solution was scanned at a λ_{max} of 785 nm for its absorbance values. A standard calibration curve was obtained by plotting values of absorbance with percentage solution. One gram of 30% SiW_{12}/MCM-41 as well as 30% SiW_{11}/MCM-41 was refluxed for 4h with 10 mL

of conductivity water. 1 mL of the supernant solution was then treated with 10% ascorbic acid. No development of blue color indicates no leaching. The same procedure was repeated with water, methanol, glycerol and also with the filtrates of all the reaction mixtures after completion of the reaction. The above procedure was followed for all catalysts and no leaching was found. For each case, absence of blue color indicates no leaching of SiW_{12}/SiW_{11} from support into reaction medium. The study indicates the presence of chemical interaction between the SiW_{12}/SiW_{11} and MCM-41, as well as stability of the resultant catalysts under reaction conditions.

Elemental Analysis

Table 2. EDS elemental analysis.

Materials	Elemental analysis (weight %)			
	Si		W	
	By EDS	Theoretical	By EDS	Theoretical
30% SiW_{12}/MCM-41	27	27	17.9	19
30% SiW_{11}/MCM-41	27.6	28	15.2	15

The EDS elemental analysis for 30% SiW_{12}/MCM-41 and 30% SiW_{11}/MCM-41 is shown in Table 2. The results obtained from EDS were in good agreement with the analytically calculated values.

Thermal Analysis

TG-DTA of MCM-41, 30% SiW_{12}/MCM-41 and 30% SiW_{11}/MCM-41 are shown in Figure 7. TGA of MCM-41 shows initial weight loss of 6.14% at 100 ^{o}C. This may be due to the adsorbed water molecules. The last 5.92% weight loss above 350 ^{o}C may be due to the condensation of silanol groups to form siloxane

bonds. After that, the absence of any weight loss shows that support is stable up to 500 ^{o}C.

The TGA of 30% SiW_{12}/MCM-41 (Figure 7) shows initial weight loss of 4–6% due to the loss of adsorbed water. Second weight loss of 2–3 % between 150 and 250 ^{o}C corresponds to the loss of water of crystallization of Keggin ion. After that another gradual weight loss was also observed from 250 to 480 ^{o}C due to the difficulty in removal of water contained in SiW_{12} molecules inside the channels of MCM-41. The results are in good agreement with the reported one [24]. Such type of inclusion causes the stabilization of SiW_{12} molecules inside the channels of MCM-41.

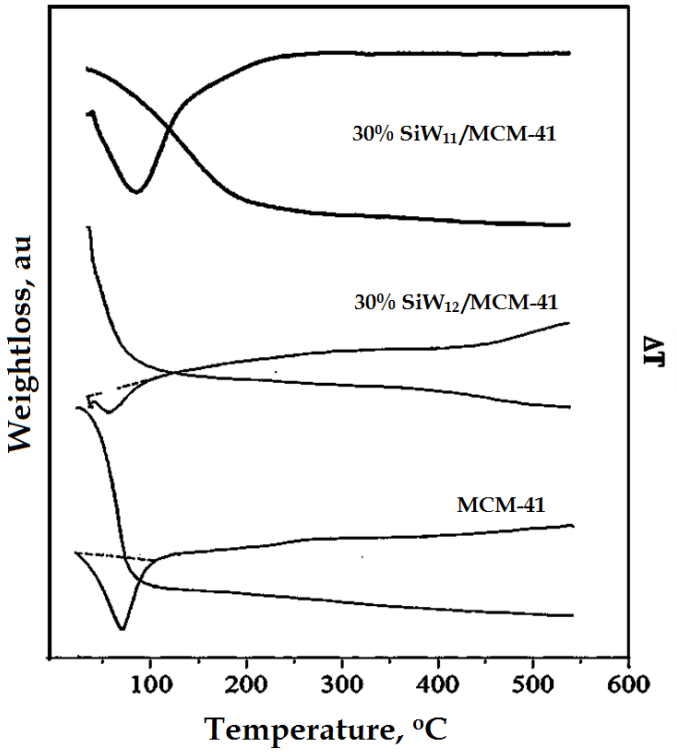

Figure 7. TG-DTA of MCM-41, 30% SiW_{12}/MCM-41 and 30% SiW_{11}/MCM-41.

The TGA of 30% SiW_{11}/MCM-41 (Figure 7) shows initial weight of 6% up to 150 ^{o}C may be due to the removal of adsorbed water molecules. Second weight loss of 2% has been observed up to 250 ^{o}C which is due to loss of water of

crystallization. No notable loss up to 400 ^{o}C indicates the stability of the catalyst up to 400 ^{o}C. The TGA data shows that anchoring of SiW_{11} on to MCM-41 increases the thermal stability of SiW_{11}.

BET Surface Area

Table 3. Textural properties of support and catalysts.

Catalyst	Surface area (m^2/g)	Pore diameter d(Å)	Mesopore volume(cm^3/g)
MCM-41	659	47.90	0.79
10% SiW_{12}/MCM-41	539	29.62	0.39
20% SiW_{12}/MCM-41	464	29.45	0.30
30% SiW_{12}/MCM-41	349	29.23	0.26
40% SiW_{12}/MCM-41	196	15.28	0.17
10% SiW_{11}/MCM-41	575	41.32	0.67
20% SiW_{11}/MCM-41	546	39.76	0.65
30% SiW_{11}/MCM-41	536	39.60	0.63
40% SiW_{11}/MCM-41	380	28.41	0.28

The values of surface area, pore size and pore volumes of support and the catalysts are presented in Table 3. The incorporation of active species inside the channels of MCM-41 leads to decrease in the surface area, pore size and pore volume of both the catalysts. The overall decrease in surface area of both the catalysts with respect to the support gives the first indication of a chemical interaction between SiW_{11}/SiW_{12} and MCM-41. However, both surface area and pore diameter of 30% SiW_{11}/MCM-41 are higher than those of 30% SiW_{12}/MCM-41. This may be due to the fact that the removal of W-O unit from

the parent SiW_{12} results in decrease in the size of SiW_{11} species leading to increase in the available space inside the channels of the support. As the % loading increases surface area, pore diameter and pore volume all strongly decreases. This confirms that the active species are located quite inside the channels of the MCM-41. Further, up to 30% loading constant decrease in the surface area was observed which may be due to the monolayer formation of the active species. Further increase in % loading leads to the drastic decrease in the surface area as well as pore diameter due to blocking of the pores by active species. As a result 30% loaded catalysts were selected for the further characterizations.

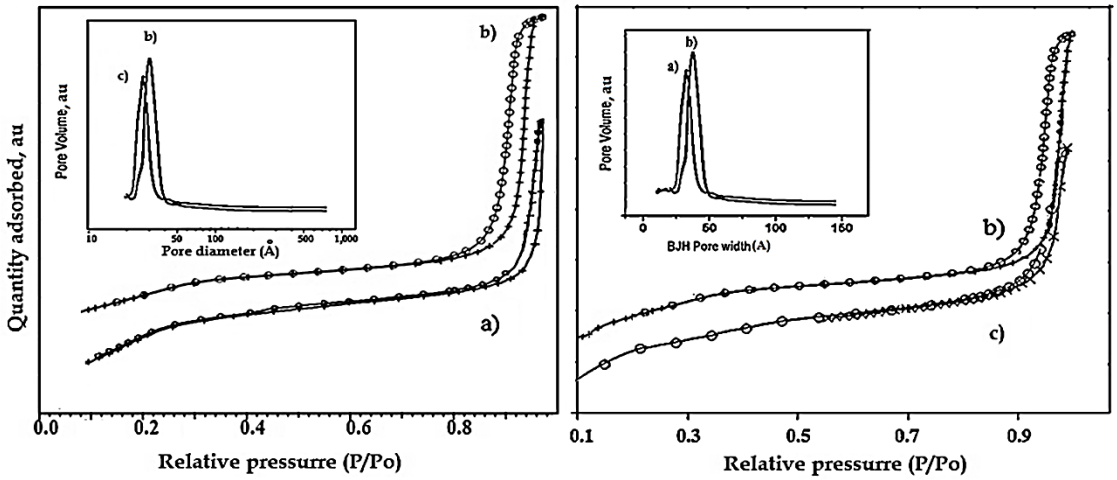

Figure 8. Nitrogen sorption isotherms and pore size distribution (inset) of a) 30% SiW_{12}/MCM-41, b) MCM-41, and c) 30% SiW_{11}/MCM-41.

The N_2 adsorption–desorption isotherms as well as pore size distributions of MCM-41, 30% SiW_{12}/MCM-41 and 30% SiW_{11}/MCM-41 are shown in Figure 8. All the N_2 adsorption–desorption isotherms are of type IV in nature according to the IUPAC classification and exhibited an H1 hysteresis loop which is a characteristic of mesoporous solids [25]. The adsorption branch of each isotherm showed a sharp inflection, which means a typical capillary condensation within uniform pores. The position of the inflection point is

clearly related to the diameter of the mesopore, and the sharpness of this step indicates the uniformity of the mesopore size distribution. The pore size distributions in the inset show that all the samples have narrow pore size distribution within the mesopore range.

FT- IR Spectroscopy

The FT-IR of MCM-41 (Figure 9) shows a broad band around 1300 and 1000 cm^{-1}, matching to asymmetric stretching of Si-O-Si. The bands at 460 and 808 cm^{-1} are attributed to the bending vibration of the Si-O-Si bonds and free silica. The band at 966 cm^{-1} corresponds to symmetric stretching vibration of Si-OH.

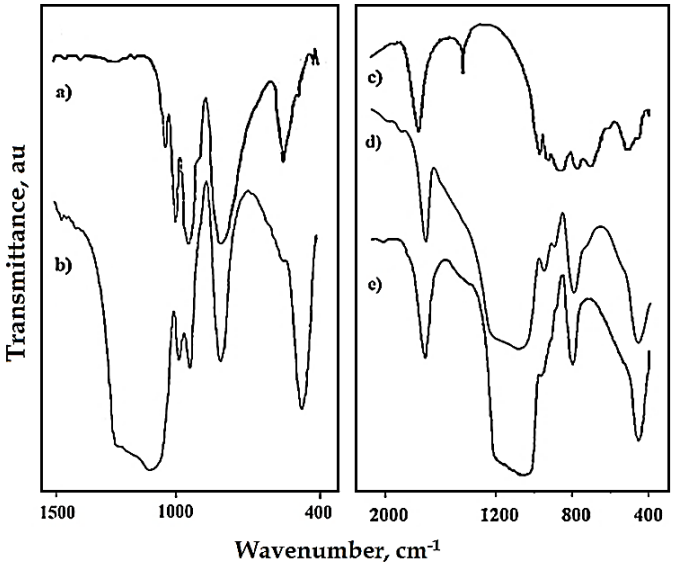

Figure 9. FT-IR spectra of a) SiW_{12}, b) 30% SiW_{12}/MCM-41, c) SiW_{11}, d) 30% SiW_{11}/MCM-41 and e) MCM-41.

The FT-IR spectrum of 30% SiW_{12}/MCM-41 (Figure 9) showed the retention of typical bands for SiW_{12}, at 979 cm^{-1} and 923 cm^{-1} corresponding to $W=O_d$ and $Si-O_a$ symmetric stretching, respectively. The FT-IR spectrum of 30% SiW_{11}/MCM-41 (Figure 9) shows bands at 960 cm^{-1} and 900 cm^{-1} corresponding to the symmetric stretching of $W=O_d$ and $Si-O_a$ bonds of SiW_{11}, respectively. Similarly, the presence of these bands confirms that structure of SiW_{12}/SiW_{11} is

intact even after impregnation to the support. The substantial shift in the bands indicates interaction between SiW_{12}/SiW_{11} and surface silanol groups of MCM-41.

FT- Raman Spectroscopy

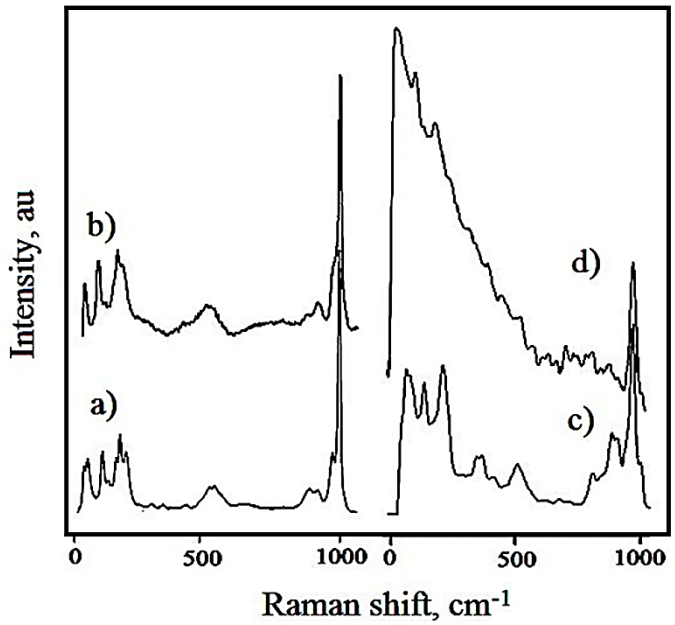

Figure 10. Raman spectra of a) SiW_{12}, b) 30% SiW_{12}/MCM-41, c) SiW_{11} and d) 30% SiW_{11}/MCM-41.

Raman spectra of both the catalysts are shown in Figure 10. The Raman spectrum of SiW_{12} shows bands at 1054, 976, 888, 565, and 208 cm^{-1} corresponding to υ_s (W-O_d), υ_{as} (W-O_d), υ_{as} (W-O_b-W), υ_s (W-O_c-W), and υ_s (W-O_a), respectively (Figure 10a). The Raman spectrum of 30% SiW_{12}/MCM-41 remains almost the same, confirming the retainment of the Keggin structure (Figure 10b). The Raman spectrum of SiW_{11} shows typical bands at 971, 890, 814, 521 and 231 cm^{-1} corresponding to υ_s (W-O_d), υ_{as} (W-O_d), υ_{as} (W-O_b-W), υ_s (W-O_c-W), and υ_s (W-O_a), respectively (Figure 10c). The presence of these bands confirms the formation of lacunary SiW_{11} species. The catalyst 30% SiW_{11}/MCM-41 showed Raman bands at 969, 879, 793 and 224 cm^{-1} with respect to υ_s (W-O_d), υ_{as} (W-O_d), υ_{as} (W-O_b-W) and υ_s (W-O_a), respectively

(Figure 10d). The presence of these bands confirms the intact SiW_{11} species in 30% SiW_{11}/MCM-41.

Furthermore, the slight shift in the Raman bands for both the catalysts indicates the chemical interaction of the active species SiW_{11}/SiW_{12} with the surface silanol groups of MCM-41. The establishment of chemical interaction was further confirmed by means of ^{29}Si MAS NMR.

^{29}Si MAS- NMR Studies

^{29}Si MAS-NMR is the most important method to study chemical environment around the silicon nuclei in mesoporous silica materials. Figure 11 shows the ^{29}Si MAS-NMR spectra of MCM-41, 30% SiW_{12}/MCM-41 and 30% SiW_{11}/MCM-41.

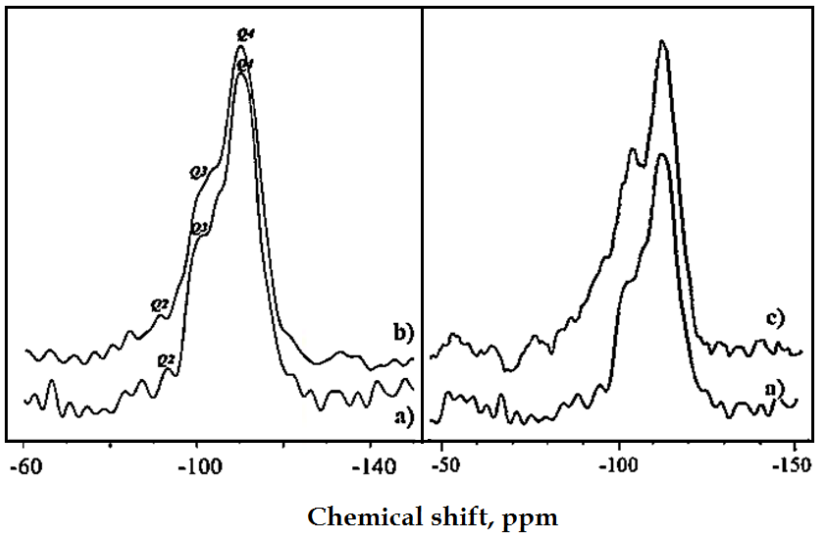

Figure 11. ^{29}Si -MAS NMR spectra of (a) MCM-41, (b) 30% SiW_{12}/MCM-41 and (c) 30% SiW_{11}/MCM-41.

A broad peak between -90 and -125 ppm was observed for the catalysts which can be attributed to three main components of MCM-41 resulted from Q^2 $Si(OSi)_2(OX)_2$, Q^3 $Si(OSi)_3(OX)$ and Q^4 $Si(OSi)_4$ where, X is H or SiW_{12}/SiW_{11} [26-27] indicating that MCM-41 retains its structure in both the catalysts. The

values of chemical shifts for the Q^x are presented in Table 4. The spectra of 30% SiW_{12}/MCM-41 and 30% SiW_{11}/MCM-41 were relatively broad and low in intensity as compared to MCM-41. This is due to the strong hydrogen bonding between SiW_{12}/SiW_{11} and Q^2 $Si(OSi)_2(OH)_2$ (surface silanol groups) of MCM-41.

Table 4. ^{29}Si chemical shifts of the catalysts.

Material	Q^2, ppm	Q^3, ppm	Q^4, ppm
30% SiW_{12}/MCM-41	-93	-103	-110
30% SiW_{11}/MCM-41	-102	-104.6	-110.5

To study the dispersion of SiW_{12}/SiW_{11} species on the support, materials were further characterized for XRD, SEM and TEM.

X-Ray Diffraction

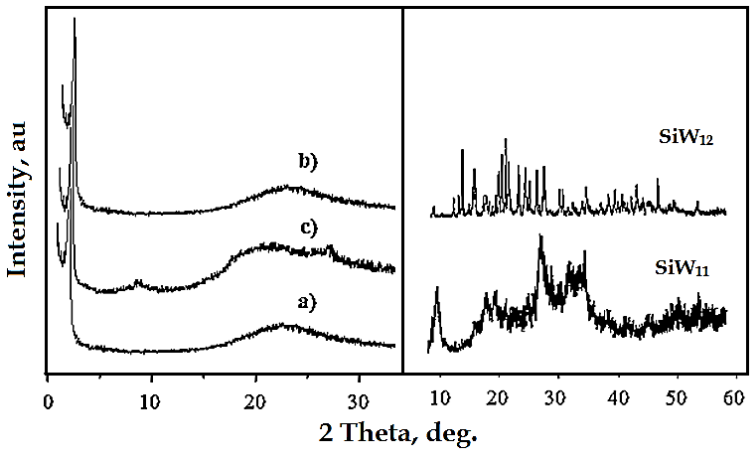

Figure 12. XRD patterns of a) MCM-41, b) 30% SiW_{12}/MCM-41 and c) 30% SiW_{11}/MCM-41.

XRD patterns of MCM-41, 30% SiW_{12}/MCM-41 and 30% SiW_{11}/MCM-41 are shown in Figure 12. The XRD pattern of the MCM-41 shows a sharp reflection

around $2\theta=2^{o}$ corresponding to (100) plane indicating well-ordered hexagonal structure of MCM-41. The comparison of the XRD patterns of MCM-41 and the catalysts reveals that the mesoporous structure of MCM-41 is rather intact even after anchoring of SiW_{12}/SiW_{11} species. Further the absence of characteristic peaks of crystalline phase of SiW_{12} as well as SiW_{11} in the respective catalysts indicates that the active species are highly dispersed inside the hexagonal channels of MCM-41.

Scanning Electron Microscopy

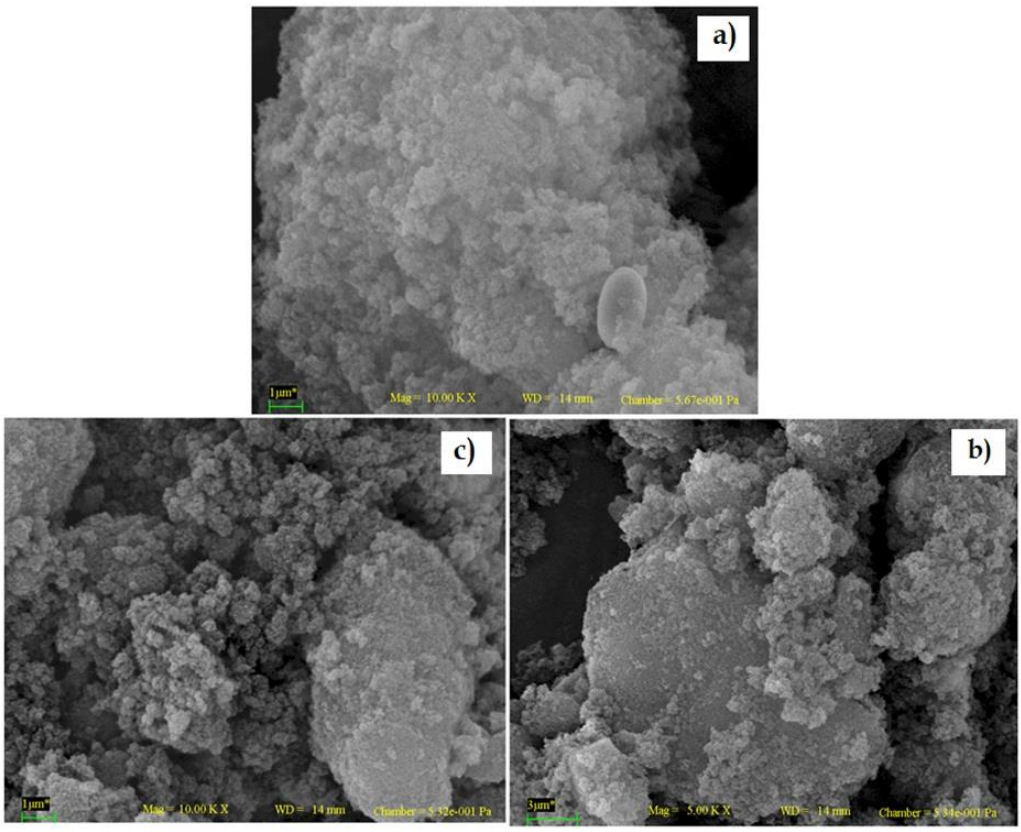

Figure 13. SEM images of a) MCM-41, b) 30% SiW_{12}/MCM-41 and c) 30% SiW_{11}/MCM-41.

SEM images of support and the catalysts are shown in Figure 13. The surface morphology of the anchored catalysts is almost identical to that of MCM-41. No change in surface morphology of the catalysts indicates that SiW_{12}/SiW_{11}

species are well dispersed inside the hexagonal pores. Further no separate crystallites of bulk phase of SiW_{12}/SiW_{11} were found in catalysts.

Transmission Electron Microscopy

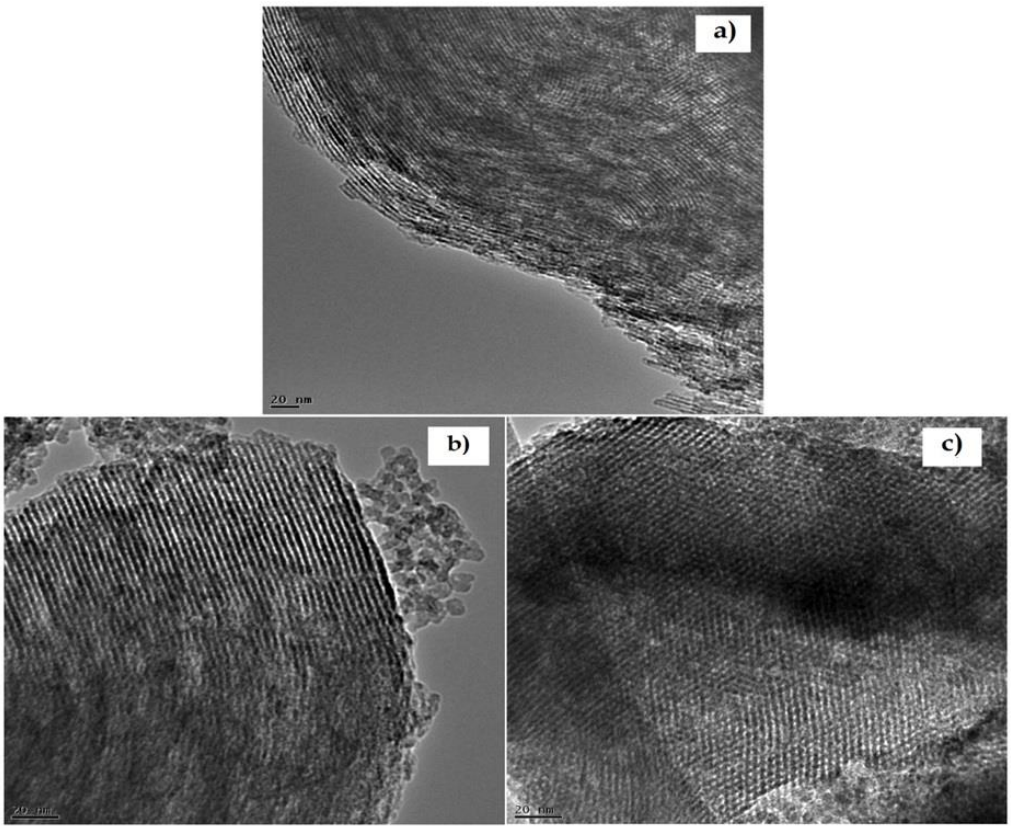

Figure 14. TEM images of a) MCM-41, b) 30% SiW_{12}/MCM-41 and c) 30% SiW_{11}/MCM-41.

TEM images of MCM-41, 30% SiW_{11}/MCM-41 and 30% SiW_{12}/MCM-41 are shown in Figure 14. The TEM image of MCM-41 (Figure 14a) displays the morphology of 2D hexagonal arrays of channels with uniform pore sizes. The TEM images of 30% SiW_{11}/MCM-41 as well as 30% SiW_{12}/MCM-41 (Figure 14b and 14c) show well-ordered hexagonal nano-channels on a large scale. The surface morphology of the support and the catalysts is almost the same, indicating that active species are well dispersed inside the hexagonal pores of MCM-41 with retention of a uniform hexagonal structure.

Acidity Measurements

According to Vasquez et al [28], the potentiometric titrations with n-butylamine enable the quantitative determination of types of acid sites of the solid acid catalysts. The acidic strength of surface sites can be assigned according to the following ranges: very strong site, Ei > 100 mV; strong site, 0 < Ei < 100 mV; weak site, -100 < Ei < 0 mV and very weak site, Ei < -100 mV.

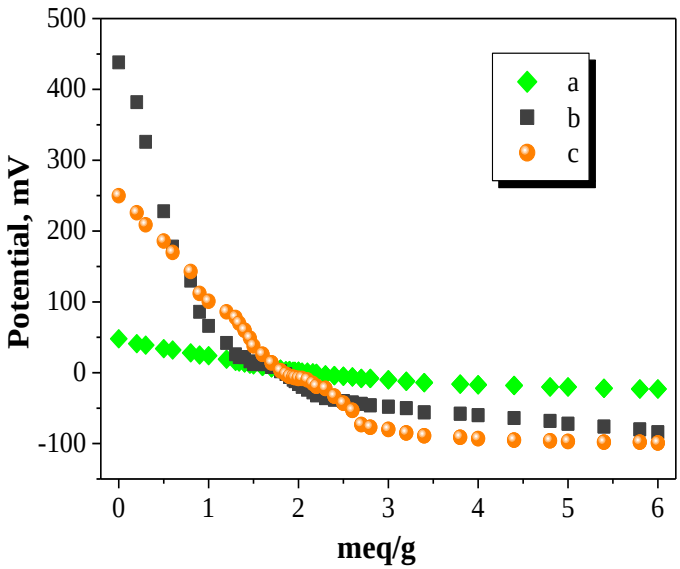

Figure 15. Potentiometric titration curves of a) MCM-41, b) 30% SiW_{12}/MCM-41 and c) 30% SiW_{11}/MCM-41.

The plots of the electrode potential as a function of meq amine/g of the catalysts are shown in Figure 15. It was observed that, both the catalysts contain very strong acid sites. The strength of acidic sites in terms of initial electrode potential is shown in Table 5. It is clear from the Table 5 that the incorporation of species SiW_{12}/SiW_{11} increases the strength of the acid sites of catalysts to a great extent. It is also interesting to note that almost all values are similar in both the catalysts except the acidic strength. The acidic strength of 30% SiW_{11}/MCM-41 is lower than that of 30% SiW_{12}/MCM-41. The reason being, the acidic character of polyoxometalates is mainly due to the acidic addenda atoms i.e. tungsten in the present case and removal of one tungsten-

oxygen unit from the parent SiW_{12} is expected to decrease the acidity of the SiW_{11}. The obtained value is in good agreement with the expected one.

Table 5. n-Butylamine potentiometric acidity of support and the catalysts.

Material	Acidic strength, mV	Types of acid sites, meq/g		Total acidic sites, meq/g
		very strong	strong	
MCM-41	48	-	2.0	2.0
30% SiW_{12}/MCM-41	438	0.9	2.5	3.4
30% SiW_{11}/MCM-41	260	0.9	2.4	3.3

Conclusions

- *Synthesis and isolation* of sodium salt of SiW_{11} was achieved successfully, and confirmed by elemental and spectral studies.
- MCM-41 was synthesized by *non-hydrothermal synthetic method*, and used for anchoring SiW_{12}/SiW_{11}. XRD and TEM confirm the formation of MCM-14 with *hexagonal long range* order in the material.
- *Thermal stability* of SiW_{12}/SiW_{11} increases after *anchoring* on to MCM-41, and catalysts, 30% SiW_{12}/MCM-41 and 30% SiW_{11}/MCM-41 were stable up to ~430 ^{o}C.
- FT-IR and Raman spectra show that *Keggin ion structure* of SiW_{12}/SiW_{11} *remains intact* even after anchoring on to MCM-41.
- BET surface area, ^{29}Si MAS-NMR data and Raman studies show that there is a *strong interaction*, hydrogen bonding, between surface oxygens of SiW_{12}/SiW_{11} with the silanol groups of MCM-41. From *spectroscopic characterization*, the possible interaction between the support and SiW_{12}/SiW_{11} is as follows,

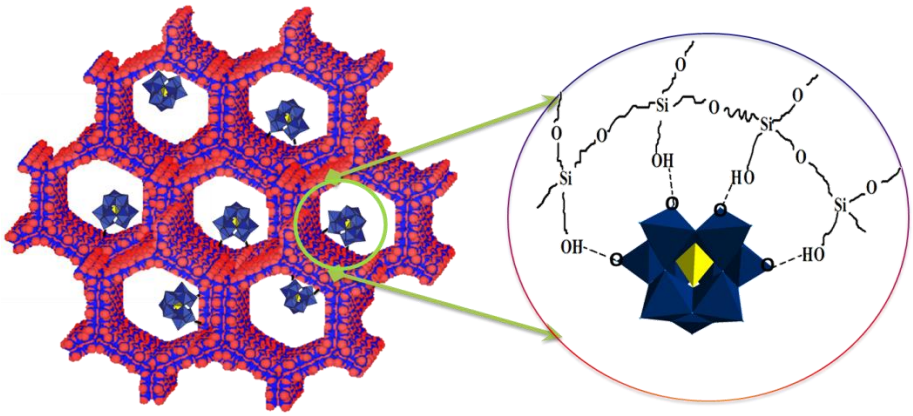

- XRD, SEM, and TEM studies reveal that both SiW_{12} and SiW_{11} are *uniformly dispersed* inside the channels without disturbing the hexagonal array of MCM-41.

References

1. V. Brahmkhatri, A. Patel, Ind. Eng. Chem. Res., 50, 13693, (2011).
2. V. Dufaud, F. Lefebvre, Materials, 3, 682, (2010).
3. Y. Yang, Y. Guo, C. Hu, E. Wang, Appl. Catal. A: Gen., 252 (2003) 305.
4. D. Li, Y. Guo, C. Hu, L. Mao, E. Wang, Appl. Catal. A: Gen., 235, 11, (2002).
5. Y. Guo, Y. Yang, C. Hu, C. Guo, E. Wang, Y. Zou, S. Feng, J. Mater. Chem., 12, 3046, (2002).
6. R. Zhang, C. Yang, J. Mater. Chem., 18, 2691, (2008).
7. C. M. Granadeiroa, A. D.S. Barbosaa, P. Silva, F. A. Almeida Pazb, V. K. Sainic, J. Piresc, B. de Castroa, S. S. Balulaa, L. Cunha-Silvaa, , Appl. Catal. A: Gen., 453, 316, (2013).
8. Q. Cai, Z.S. Luo, W. Q. Pang, Y. W Fan, X. H. Chen, F. Z. Cui, Chem. Mater. 13, 258 (2001)
9. C. Brevard, R. Schimpf, G. Tourne, C. Tourne, J. Am. Chem. Soc., 105 7059, (1983).
10. J. M. Thomas, W. J. Thomas, Principles and Practice of Heterogeneous Catalysis, VCH, Weinheim, (1997).
11. R. A. van Santen, P. W. N. M. Van Leeuwen, J. A. Moulijin, B. A. Averil (Eds.), Catalysis: An Integrated Approach, (2nd ed.), Elsevier, Amsterdam, (1999).
12. R. Richards (Eds.), "Surface and Nanomolecular Catalysis", CRC press, Ch. 1, p2, (2006).
13. J. L. G. Fierro, Spectroscopic Characterization of Heterogeneous Catalysts, Stud. Surf. Sci. Cat., Elsevier, vol. 57A, (1990).
14. D. Skoog, F. Holler, T. Nieman, "Principles of Instrumental Analysis", 5th ed., (2001).
15. J. H. Clark, A. P. Kybett, D. J. Maequarrie, Supported reagents: preparation, analysis and application, VCH Inc. New York (1992).

16. D. J. Gardiner, Practical Raman spectroscopy. Springer-Verlag (1989).
17. N. Gupta, V. Kartha, R. Rajadhyaksha, Spectroscopic methods in heterogeneous catalysis, Tata McGraw Hill, (1989).
18. J. Mayer, L. A. Giannuzzi, T. Kamino, J. Michael. TEM Sample Preparation and FIB-Induced Damage. Mrs Bulletin, vol. 32 (2007).
19. P. Ferreira, I. M. Fonseca, A. M. Ramos, J. Vital, J. E. Castanheiro, Appl, Catal. B, 98, 94 (2010).
20. N. Legagneux, J. M. Basset, A. Thomas, F. Lefebvre, A. Goguet, J. Sa, C. Hardacre, Dalton. Trans., 2235, (2009).
21. Y. Yang, Y. Guo, C. Hu and E. Wang, Appl. Catal. A: Gen., 252, 305, (2003).
22. L. C. Moura, J. G. Eon, S. Caldarelli, S. Paul, Ann. Magn. Reson., 4, 86, (2005).
23. G. D. Yadav, V. V. Bokade, Appl. Catal. A Gen., 147, 299, (1996).
24. G. Kamalakar, K. Komura, Y. Kubota, Y. Sugi, J. Chem. Technol. Biotechnol. 81, 981 (2006).
25. Y. Luo, Z. Hou, R. Li, X. Zheng, Micropor. Mesopor. Mater. 109, 585 (2008).
26. R.C. Schroden, C.F. Blanford, B.J. Melde, B.J.S. Johnson, A. Stein, Chem. Mater. 13 ,1074 (2001).
27. W.H. Zhang, J. Lu, B. Han, M. Li, J. Xiu, P. Ying, C. Li, Chem. Mater. 14, 3413 (2002).
28. P. Vazquez, L. Pizzio, C. Caceres, M. Blanco, H. Thomas, E. Alesso, L. Finkielsztei, L. Lantano, G. Moltrasio, J. Aguirre, J. Mol. Catal. A: Chem., 161, 223 (2000).